

19. The coordination geometry of CuA is also consistent with square planar geometry, but absorption edge features strongly associated with square planar geometry are absent in XAS data from oxidized PHM (20).
20. J. S. Boswell, B. J. Reedy, R. Kulathila, D. Merkler, N. J. Blackburn, *Biochemistry* **35**, 12241 (1996).
21. B. J. Reedy and N. J. Blackburn, *J. Am. Chem. Soc.* **116**, 1924 (1994).
22. The coordination of CuA may include two solvent ligands, in addition to the three histidines. Many proteins in the Protein Data Bank [T. Bernstein *et al.*, *J. Mol. Biol.* **112**, 535 (1977)] contain Cu binding sites composed solely of histidine and solvent ligands (for example, Cu or Zn superoxide dismutase, ascorbate oxidase, and hemocyanin). All of these Cu sites are molecular oxygen acceptors, either for oxidoreductase activity or oxygen transport. The coordination of CuB is most similar to type I Cu sites, which are typically composed of two histidines, one methionine, and one cysteine (for example, cupredoxins, ascorbate oxidase, ceruloplasmin, and Cu nitrite reductase). Type I Cu sites function as electron transfer sites. As observed in PHMcc, the bond length of the Cu-methionine bond in type I Cu sites is long (2.4 to 3.4 Å).
23. This iodinated tyrosylglycine is an effective substrate of PHMcc ($K_m \approx 3 \mu\text{M}$).
24. EXAFS experiments with reduced, anaerobic PAM found that M314 became more rigid (lower Debye-Waller factor) upon binding of peptidylglycine substrate (20).
25. J. P. Klinman, *Chem. Rev.* **96**, 2541 (1996).
26. T. M. Zabriske, H. Cheng, J. C. Vederas, *J. Chem. Soc. Chem. Commun.*, 571 (1991).
27. D. J. Merkler, R. Kulathila, D. E. Ash, *Arch. Biochem. Biophys.* **317**, 93 (1995); J. S. Kizer *et al.*, *Endocrinology* **25**, 2262 (1986); S. E. Ramer, H. Cheng, M. M. Palcic, J. C. Vederas, *J. Am. Chem. Soc.* **110**, 8526 (1988); D. Ping, A. G. Katopodis, S. W. May, *ibid.* **114**, 3998 (1992); P. F. Fitzpatrick and J. J. Villafranca, *J. Biol. Chem.* **261**, 4510 (1986); A. R. Battersby, P. W. Sheldrake, J. Staunton, D. C. Williams, *J. Chem. Soc. Perkin I*, 1056 (1976).
28. S. M. Miller and J. P. Klinman, *Biochemistry* **24**, 2114 (1985).
29. M. C. Brenner and J. P. Klinman, *ibid.* **28**, 4664 (1989).
30. This pH corresponds to the pH optimum of rat PHM (2, 7) and also is the pH of the crystallization buffers used for the structures described in this work.
31. Failure of glycyllamides to be substrates cannot be attributed to loss of the substrate-R240 salt bridge. Mutation of R240 to glutamine in PHMcc yields an active enzyme with a 2-fold increase in K_m and a 200-fold decrease in V_{max} (37). R240 is conserved among PHM sequences; in DBM sequences, R240 is replaced by a conserved glutamine.
32. E. I. Solomon, U. M. Sundaram, T. E. Machonkin, *Chem. Rev.* **96**, 2563 (1996).
33. K. D. Karlin, *Science* **261**, 701 (1993).
34. Crude modeling indicates that interdomain motion in PHMcc could be of two types: hinge motion and shear motion. Hinge motion brings CuA and CuB no closer than 8 Å, but creates new interdomain contacts that may facilitate electron transfer. Shear motion is required to further reduce the distance between CuA and CuB, but in doing so, the interdomain interfaces become increasingly mismatched.
35. R. A. Scott, R. J. Sullivan, W. E. DeWolf Jr., R. E. Dolle, L. I. Kruse, *Biochemistry* **27**, 5411 (1988).
36. M. D. Newton, *J. Electroanal. Chem.* **5025**, 1 (1997); *Chem. Rev.* **91**, 767 (1991).
37. S. T. Prigge, A. S. Kolhekar, B. A. Eipper, R. E. Mains, L. M. Amzel, data not shown.
38. Z. Otwinowski, in *Data Collection and Processing*, L. Sawyer, N. Isaacs, S. Bailey, Eds. (Science and Engineering Research Council, Daresbury Laboratory, Warrington, UK, 1993), pp. 56–62.
39. A. T. Brünger, *X-PLOR, Version 3.1: A System for X-ray Crystallography and NMR* (Yale Univ. Press, New Haven, CT, 1992).
40. Cells were grown in an atmosphere of 5% CO₂ at 37°C in 2-liter roller bottles in 250 ml of α -MEM (minimum essential medium) with 10% fetal calf serum. Six roller bottles were used to produce PHMcc; the most successful culture was harvested for 60 days and produced over 0.75 mg of PHMcc per day during peak production. PHMcc was purified in batches of 4 to 6 liters with three main steps: (NH₄)₂SO₄ precipitation, FPLC (fast-protein liquid chromatography) Phenylsuperose chromatography, and FPLC MonoQ chromatography (10). Concentration yielded 1.5 ml of PHMcc solution that was >95% pure on the basis of Coomassie brilliant blue staining of SDS-polyacrylamide gels and had an absorbance at 280 nm (A_{280}) of 20 units.
41. Crystallization conditions of 525 μM cupric sulfate, 3.08 mM NaNO₃, 100 mM dimethylarsinic acid (pH 5.5) at 25°C produced crystals of final dimensions 0.4 mm by 0.1 mm by 0.1 mm over 2 to 4 weeks. Crystals were enlarged to dimensions of 0.8 mm by 0.2 mm by 0.2 mm through macroseeding.
42. Beamline X4A at the National Synchrotron Light Source (NSLS), a U.S. Department of Energy (DOE) facility, is supported by the Howard Hughes Medical Institute. The Stanford Synchrotron Radiation Laboratory (SSRL) is funded by the DOE, Office of Basic Energy Sciences. The Biotechnology Program is supported by the NIH, Biomedical Research Technology Program, Division of Research Resources. Further support is provided by the DOE, Office of Health and Environmental Research.
43. Diffraction data were collected on Fuji HR-5 phosphorimaging plates and digitized with a Fuji offline scanner. Data were collected from a single crystal cryopreserved in buffer [200 μM CuSO₄, 100 mM dimethylarsinic acid, 30% (v/v) glycerol] and flash frozen in a 1-mm loop of 11 gauge ethylon surgical fiber in a stream of nitrogen gas (100 K). Four data sets were collected at different x-ray energies at or near the K absorption edge of Cu with the crystal oriented such that Bijvoet pairs could be collected simultaneously. The four data sets were collected in parallel in groups of four 150-s exposures to minimize scaling problems between the data sets.
44. W. A. Hendrickson, *Science* **254**, 51 (1991).
45. The Cu anomalous signal was enhanced by the presence of a third Cu (from the crystallization conditions) at a crystal contact site.
46. Collaborative Computation Project 4, *Acta Crystallogr.* **D50**, 760 (1994).
47. A. T. Jones, J. Y. Zou, S. W. Cowan, M. Kjeldgaard, *ibid.* **A47**, 110 (1991).
48. High-resolution data were collected on an *R*-axis IIc detector with CuK α radiation from a Rigaku RU200 rotating anode and processed in DENZO and SCALEPACK (38).
49. The substrate (*N*- α -acetyl-3,5-diodotyrosylglycine) was synthesized by solid-support peptide synthesis with preiodinated tyrosine (Bachem). The substrate was solubilized at a concentration of 1 mg/ml in 10% glycerol and soaked into a PHMcc crystal for 2 hours before data collection. Diffraction data were collected on an *R*-axis IV detector with CuK α radiation from a Rigaku RU200 rotating anode and processed in DENZO and SCALEPACK (38). The PHMcc-substrate complex crystal was isomorphous to native crystals, allowing a difference electron density map ($F_{\text{complex}} - F_{\text{native}}$) to be calculated with native phases. The substrate iodine positions were deduced from this map contoured at 7σ and the other substrate atoms were built into lower levels of difference density. The PHMcc-substrate structure was refined in X-PLOR-3.8 (39) beginning with native phases.
50. S. V. Evans *J. Mol. Graphics* **11**, 268 (1993).
51. We thank C. Ogata and the staff at beamline X-4A for assistance during data collection at the NSLS; H. Bellamy and P. Phizackerly for assistance during data collection at beamline 1-5 at the SSRL; Y. Pan, S. Gabelli, M. Bianchet, K. Lee, G. Bains, M. Faig, D. Medjahed, and K. Doctor for assistance during synchrotron data collection; T. Hand for constructing the R240Q mutant; H. Wu and the Hendrickson group for the MADSYS suite of programs; and D. Leahy, J. Berg, and A. Milovan for discussions or critical review of this manuscript. Supported by NIH grants DK32949 (B.A.E and R.E.M.) and GM44692 (L.M.A.). The coordinates for PHMcc have been deposited in the Protein Data Bank (accession number 1PHM).

18 August 1997; accepted 7 October 1997

Requirement for the CD95 Receptor-Ligand Pathway in c-Myc-Induced Apoptosis

Anne-Odile Hueber,* Martin Zörnig, Debbie Lyon, Takashi Suda, Shigekazu Nagata, Gerard I. Evan*

Induction of apoptosis by oncogenes like *c-myc* may be important in restraining the emergence of neoplasia. However, the mechanism by which *c-myc* induces apoptosis is unknown. CD95 (also termed Fas or APO-1) is a cell surface transmembrane receptor of the tumor necrosis factor receptor family that activates an intrinsic apoptotic suicide program in cells upon binding either its ligand CD95L or antibody. *c-myc*-induced apoptosis was shown to require interaction on the cell surface between CD95 and its ligand. *c-Myc* acts downstream of the CD95 receptor by sensitizing cells to the CD95 death signal. Moreover, IGF-I signaling and Bcl-2 suppress *c-myc*-induced apoptosis by also acting downstream of CD95. These findings link two apoptotic pathways previously thought to be independent and establish the dependency of *Myc* on CD95 signaling for its killing activity.

Most human tumors have genetic alterations in *myc* proto-oncogene family members that result in deregulation of *myc* expression (1). However, growth-promoting oncogenes like *c-myc* are also effective inducers of apoptosis, and this lethal attribute may both restrain inappropriate cell growth and maintain normal tissue homeostasis (2). Nevertheless, the molecular mechanism by

which the *c-myc* gene product, the transcription factor *c-Myc*, triggers the cell death program remains unknown. In contrast, the mechanism of induction of apoptosis by the transmembrane receptor CD95, which belongs to the tumor necrosis factor (TNF) receptor family, is relatively well characterized (3). Upon ligation by its ligand CD95L, a member of the TNF family, CD95 initiates

a series of intracellular events, such as activation of a cascade of cysteine proteases called caspases (4), that lead to suicide of the affected cell (5, 6). This killing activity plays a major role in the deletion of autoreactive lymphocytes and maintenance of peripheral tolerance and immunologically privileged sites (3, 5, 6). Given the ability of deregulated c-Myc to induce apoptosis, we investigated the possibility that cell killing by c-Myc and CD95 might share some common mechanisms; specifically, whether induction of apoptosis by one of these molecules might be dependent on activation of the other.

Mouse primary embryo fibroblasts (MEFs) and immortalized Swiss 3T3 (S3T3) fibroblasts expressed surface CD95 receptor (Fig. 1A) whose ligation by an agonistic antibody induced apoptotic cell death in a dose-dependent manner (Fig. 1B). Thus, an intact CD95 apoptotic signaling pathway is present in these mesenchymal cells. Both MEF and S3T3 cells also expressed low but detectable amounts of CD95 ligand (CD95L) (Fig. 1C). To examine any involvement of CD95 signaling in apoptosis induced by c-Myc, we used S3T3 cells that expressed a conditional 4-hydroxytamoxifen (OHT)-dependent c-Myc protein (S3T3 c-MycER) (7) and that die by apoptosis upon c-Myc activation in low serum concentration (8). When S3T3 c-MycER cells were incubated either with a monoclonal antibody to CD95L (CD95L mAb) that neutralizes CD95L (Fig. 2A) or with a CD95-Fc chimeric molecule that binds to CD95L and prevents its interaction with endogenous cell surface CD95 (9), c-Myc-induced apoptosis was reduced and delayed in a concentration-dependent manner (Fig. 2B). Thus, efficient induction of apoptosis by c-Myc required surface expression of CD95L.

To determine whether CD95 has a direct role in c-Myc-induced cell death, we blocked CD95 effector functions by expressing a dominant-negative mutant of the intracellular Fadd (also called MORT1) death-domain adapter protein (DN Fadd) in S3T3 c-MycER fibroblasts (10–12). This DN Fadd mutant can interact with CD95 but not the apoptosis effector caspase 8; DN Fadd thereby prevents activation of the apoptotic caspase cascade (13, 14). Expression of DN Fadd in S3T3 c-MycER cells blocked, with similar efficacy, apoptosis induced either by CD95 ligation or by c-Myc (Fig. 2C). Thus, CD95 action was required in effective cell killing by c-Myc. We con-

clude that efficient c-Myc-induced apoptosis requires cell-surface interaction between CD95 receptor and its ligand CD95L.

lpr and *gld* mice harbor inactivating mutations in the genes encoding CD95 and CD95L, respectively (15, 16). Fibroblasts from such animals might be expected to exhibit greater resistance to c-Myc-induced apoptosis because of their impaired CD95 signaling system. Accordingly, cells transiently infected with a retroviral c-mycER expression vector were exposed to low serum concentrations, and c-Myc was activated by addition of OHT. Activation of c-Myc increased the rate of apoptosis in wild-type (WT) MEFs; in contrast, *lpr* and *gld* MEFs showed no increased apoptosis after c-Myc activation (Fig. 2D). This result confirmed that surface expression of both CD95 and CD95L were necessary for efficient induction of apoptosis by deregulated c-Myc. These data are also consistent with, and explain, the previous observation that the *lpr* mice exhibit accelerated tumorigenesis in response to transgenic lymphocyte expression of the oncogene *L-myc*, a close relative of *c-myc* (17).

To investigate how c-Myc recruits the CD95-CD95L killing pathway, we made use of the Rat-1 fibroblast cell line, which harbors the c-mycER construct. These fibroblasts expressed CD95 (18) but were refractory to CD95-induced apoptosis. Nonethe-

less, they became sensitive to killing by a soluble CD95 ligand molecule upon expression of activated c-Myc (Fig. 3A). Thus, at least in part, c-Myc acts downstream of CD95 by sensitizing cells to the death pathway resulting from interaction between CD95 and its ligand.

Induction of apoptosis by c-Myc in fibroblasts is suppressed by the survival factor insulin growth factor-IGF-I (8). Although some details of the anti-apoptotic signaling pathway activated by IGF-I are emerging (19), it remains unclear at what point the survival signals interfere with the apoptotic program. Having shown that CD95-CD95L participates in c-Myc-induced apoptosis, we examined the stage at which IGF-I-mediated inhibition of apoptosis acts relative to the CD95-CD95L interaction. We therefore used an agonistic antibody to CD95 to activate CD95 on serum-deprived S3T3 fibroblasts, either in the presence or absence of IGF-I. IGF-I decreased the rate and extent of apoptosis induced by CD95 ligation (Fig. 3B); fetal calf serum (FCS) was even more efficient than pure IGF-I (18), consistent with the fact that serum contains multiple mesenchymal survival factors in addition to IGF-I (8). As the anti-apoptotic action of Bcl-2 functionally maps very close to that of the IGF-I signal in the kinetics of apoptosis (20) and because of the death-suppressing effect of

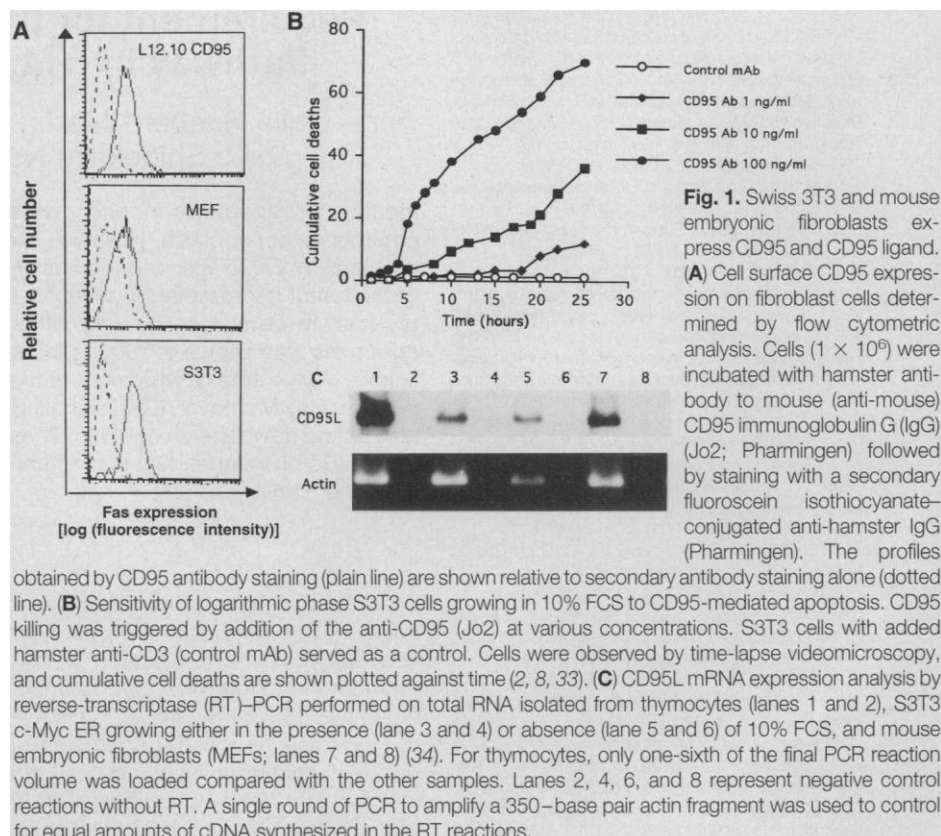


Fig. 1. Swiss 3T3 and mouse embryonic fibroblasts express CD95 and CD95 ligand. (A) Cell surface CD95 expression on fibroblast cells determined by flow cytometric analysis. Cells (1×10^6) were incubated with hamster antibody to mouse (anti-mouse) CD95 immunoglobulin G (IgG) (Jo2; Pharmingen) followed by staining with a secondary fluorescein isothiocyanate-conjugated anti-hamster IgG (Pharmingen). The profiles

obtained by CD95 antibody staining (plain line) are shown relative to secondary antibody staining alone (dotted line). (B) Sensitivity of logarithmic phase S3T3 cells growing in 10% FCS to CD95-mediated apoptosis. CD95 killing was triggered by addition of the anti-CD95 (Jo2) at various concentrations. S3T3 cells with added hamster anti-CD3 (control mAb) served as a control. Cells were observed by time-lapse videomicroscopy, and cumulative cell deaths are shown plotted against time (2, 8, 33). (C) CD95L mRNA expression analysis by reverse-transcriptase (RT)-PCR performed on total RNA isolated from thymocytes (lanes 1 and 2), S3T3 c-Myc ER growing either in the presence (lane 3 and 4) or absence (lane 5 and 6) of 10% FCS, and mouse embryonic fibroblasts (MEFs; lanes 7 and 8) (34). For thymocytes, only one-sixth of the final PCR reaction volume was loaded compared with the other samples. Lanes 2, 4, 6, and 8 represent negative control reactions without RT. A single round of PCR to amplify a 350-base pair actin fragment was used to control for equal amounts of cDNA synthesized in the RT reactions.

A.-O. Hueber, M. Zörnig, D. Lyon, G. I. Evan, Imperial Cancer Research Fund (ICRF) Laboratories, 44 Lincoln's Inn Fields, London WC2A 3PX, UK.

T. Suda and S. Nagata, Department of Genetics, Osaka University Medical School, 2-2 Yamadaoka, Suita, Osaka 565, Japan.

*To whom correspondence should be addressed. E-mail: hueber@icrf.icnet.uk and evan@icrf.icnet.uk

Bcl-2 on c-Myc-induced apoptosis (21), we examined the effect of Bcl-2 in CD95-induced apoptosis. As reported previously (22, 23), expression of Bcl-2 protein in S3T3 c-MycER cells blocked apoptosis induced by antibody to CD95 (Fig. 3C). Thus, the main anti-apoptotic signaling pathway triggered by IGF-I or by the anti-apoptotic Bcl-2 protein interferes with c-Myc-induced apoptosis downstream of the CD95-CD95L interaction, a conclusion consistent with our finding that c-Myc also acts downstream of CD95-CD95L by sensitizing the cell to apoptotic CD95 signaling.

Our data argue for the requirement of an autocrine CD95-dependent signaling mechanism in the induction of apoptosis by the

oncogene *c-myc* and suggest that the proto-oncogene *c-myc* serves to promote the efficacy with which the cell death signal arising from this autocrine CD95-CD95L interaction engages the cell's apoptotic machinery. The autocrine interaction between CD95 and CD95L must occur on the cell surface because it is disrupted by cell-impermeable blocking agents added to intact cells. Given the low level of CD95L present on the surface of the investigated cell lines the autocrine CD95 death signal is likely to be weak compared with that induced upon ligation by exogenous CD95L, as happens during T cell killing or upon experimental activation of CD95. This finding probably explains why both IGF-I signaling and Bcl-2 afford good

protection from c-Myc-induced apoptosis yet are equivocal suppressors of classical CD95-induced apoptosis.

Precedent exists for a functional relation between c-Myc and CD95 signaling. Activation-induced T cell death, which is mediated through the CD95 signaling pathway (24), exhibits a requirement for c-Myc function (25, 26). However, the exact mechanism by which c-Myc triggers death via CD95-CD95L remains obscure. c-Myc is a basic helix-loop-helix-Zip transcription factor, and site-directed mutagenesis studies indicate that c-Myc promotes apoptosis by transcriptional modulation of target genes (2, 27). Although a component of c-Myc-induced apoptosis probably acts through

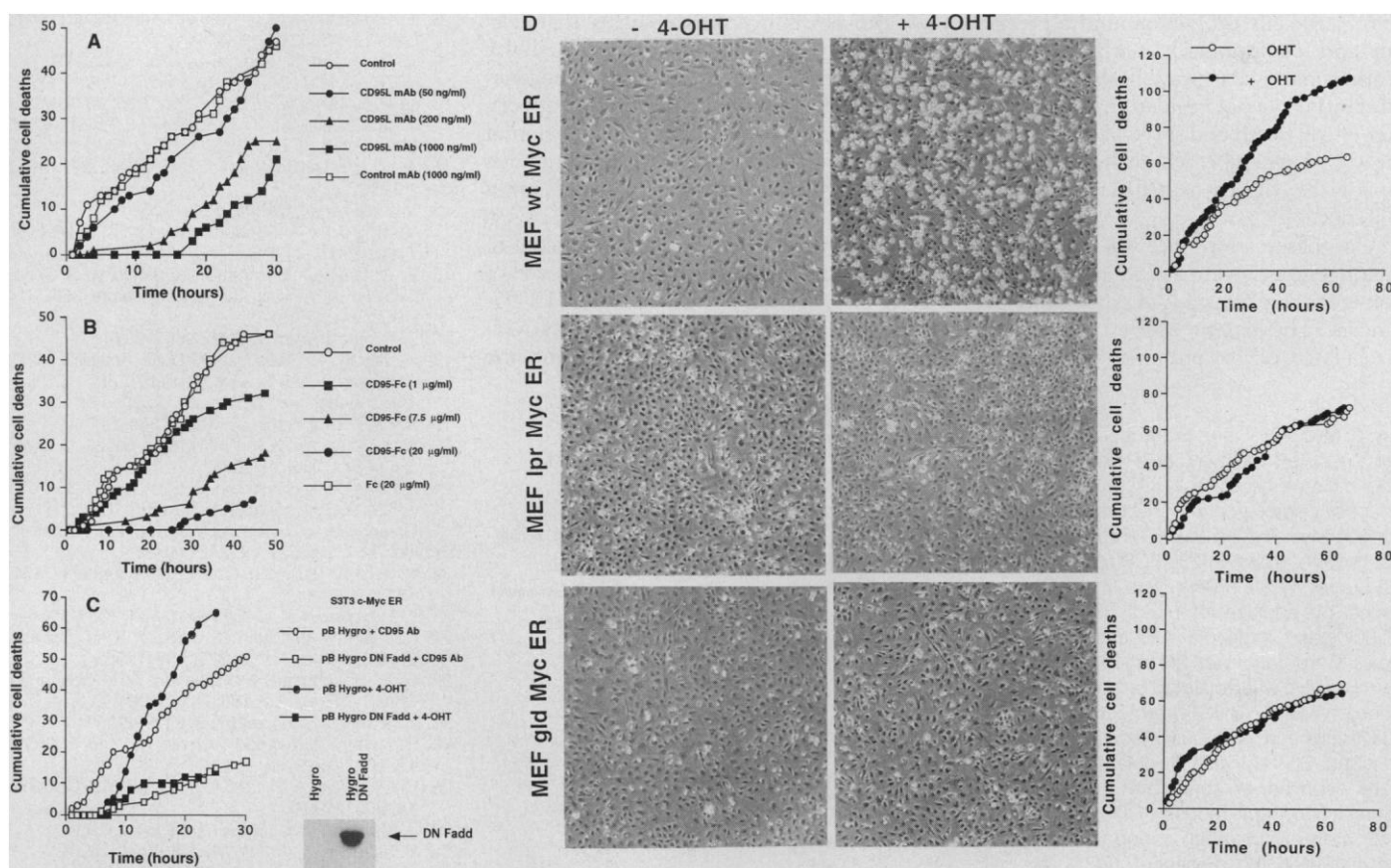


Fig. 2. Myc killing requires the CD95 pathway. **(A)** c-Myc-induced apoptosis is blocked by an anti-CD95 ligand. S3T3 MycER fibroblasts were serum-deprived for 48 hours, and c-Myc was then activated by addition of 4-hydroxy-tamoxifen (4-OHT, 100 nM; Research Biochemicals International). Cells were simultaneously treated either with or without various concentrations of a hamster mAb specific for mouse CD95 ligand (CD95L mAb) (35) and analyzed by time-lapse videomicroscopy (33). Cells treated with an isotypically matched hamster anti-mouse CD3 (control mAb) and cells incubated with no antibody served as controls. **(B)** c-Myc-induced apoptosis is blocked by a chimeric CD95-Fc molecule. S3T3 MycER fibroblasts were treated and analyzed as in (A) after incubation with various concentrations of a chimeric mouse CD95-human Fc molecule (CD95-Fc) (9). One control consisted of cells treated with human Fc alone (Fc; Jackson ImmunoResearch Labs) to determine any effect exerted by the human Fc part of the CD95-Fc molecule. The other control consisted of untreated cells. **(C)** Expression of dominant-negative Fadd protects S3T3 MycER

cells from Myc- and CD95-induced apoptotic cell death. S3T3 MycER cells expressing the pBabe Hygro vector alone (Hygro) or DN Fadd (Hygro DN Fadd) were analyzed by time-lapse videomicroscopy for sensitivity to CD95- and c-Myc-induced death (36). Expression of DN Fadd in transfected cells was confirmed by protein immunoblot analysis whereas expression of the human DN Fadd was determined by immunoprobings with a mouse anti-human Fadd (Transduction Laboratories). CD95 killing was initiated by addition of anti-mouse CD95 (Jo2) at 100 ng/ml in the presence of 10% FCS. c-Myc-induced apoptosis was induced as described in (A). **(D)** *lpr* and *gld* MEFs are resistant to c-Myc-induced apoptosis. MEFs from wild-type, *lpr*, and *gld* mice transiently expressing c-MycER (37) were cultured in medium containing 0.5% FCS in the absence (- 4-OHT) or presence (+ 4-OHT) of hydroxytamoxifen. Cultures were inspected microscopically 72 hours after infection, and representative photographs were taken. For each cell type, a time-lapse videomicroscopy analysis of cell death was performed (right column).

sensitization of cells to CD95 signals, c-Myc may also act upstream of CD95L and CD95 by inducing expression of their cognate genes. However, changes in CD95 expression after c-Myc activation were not detected in the cell lines used (18). Thus, although we cannot exclude the possibility that Myc may also operate through enhancement of CD95L expression, our data favor the idea that Myc acts by sensitizing the cell to CD95-induced apoptosis, as it does to apoptosis induced by DNA and physical damage, inhibitors of macromolecular synthesis, and TNF (28, 29).

That both the promotion of apoptosis by c-Myc and its suppression by IGF-I and Bcl-2 signaling act downstream of CD95 ligation may reflect the fact that the "sophisticated" anti-neoplastic requirements of vertebrate cells evolved around a preexisting and evolutionarily early CD95-type death signaling pathway. It also shows that substantial tiers of regulation and modulation of cell death and survival exist distal to the CD95 receptor, whose ligation can in no way be viewed as an inevitable death sentence.

Our observations are also relevant to tumorigenesis, given the ubiquitous activation and overexpression of c-Myc in human cancers. The potent apoptotic activity of deregulated c-Myc presumably means that

tumors can arise only after acquisition of compensatory anti-apoptotic mutations. This is the key to the mechanism of oncogenic synergy between c-Myc and Bcl-2. Bcl-2 suppresses c-Myc-induced apoptosis while leaving the proliferative action of c-Myc unaffected (21). Similarly, blockade of CD95 signaling by CD95L mAb or CD95-Fc in vitro blocks apoptosis but causes no detectable inhibition of cell proliferation (18). Such cells do not appear morphologically transformed, but neither do *lpr* and *gld* primary fibroblasts expressing deregulated c-Myc or fibroblasts that coexpress both c-Myc and Bcl-2 (21). It appears that cooperation between c-Myc and suppressors of apoptosis is distinct from the classical type of oncogene cooperation observed between c-Myc and activated Ras.

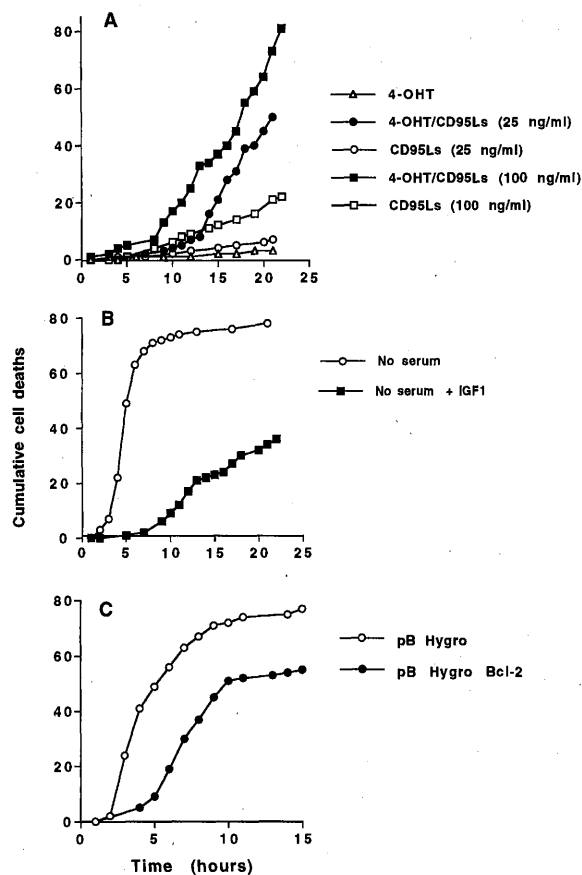
The possibility thus emerges that dysfunctions in the CD95 signaling pathway can cooperate with c-Myc in carcinogenesis. Indeed, oncogenic cooperation between the absence of CD95 and overexpression of myc has been reported in vivo (17) and is consistent with emerging evidence for a possible role of CD95 and CD95L as a tumor suppressor, not necessarily linked to the immune system (30, 31). Many tumor cells exhibit loss of sensitivity to CD95-mediated apoptosis. In addition to providing a mechanism of escape from immune

surveillance (30, 31), our studies suggest that resistance to CD95 killing may also be a mechanism by which oncogene-induced apoptosis is suppressed. Dysfunctions in cell suicide pathways mediated by CD95, together with its relatives, may therefore well prove widespread in neoplasia and could offer useful targets for molecular therapy.

REFERENCES AND NOTES

1. C. A. Spencer and M. Groudine, *Adv. Cancer Res.* **56**, 1 (1991).
2. G. I. Evan *et al.*, *Cell* **69**, 119 (1992).
3. S. Nagata, *ibid.* **88**, 355 (1997).
4. E. S. Alnemri *et al.*, *ibid.* **87**, 171 (1996).
5. S. Nagata and P. Golstein, *Science* **267**, 1449 (1995).
6. S. Nagata, *Nature Med.* **2**, 1306 (1996).
7. T. D. Littlewood, D. C. Hancock, P. S. Daniellian, M. G. Parker, G. I. Evan, *Nucleic Acids Res.* **23**, 1686 (1995).
8. E. A. Harrington, M. R. Bennett, A. Fanidi, G. I. Evan, *EMBO J.* **13**, 3286 (1994).
9. T. Suda and S. Nagata, *J. Exp. Med.* **179**, 873 (1994).
10. M. P. Boldin *et al.*, *J. Biol. Chem.* **270**, 387 (1995).
11. A. M. Chinnaiyan, K. O'Rourke, M. Tewari, V. M. Dixit, *Cell* **81**, 505 (1995).
12. A. M. Chinnaiyan *et al.*, *J. Biol. Chem.* **271**, 4961 (1996).
13. M. Muzio *et al.*, *Cell* **85**, 817 (1996).
14. M. P. Boldin, T. M. Goncharov, Y. V. Golstev, D. Wallach, *ibid.*, p. 803.
15. R. Watanabe-Fukunaga, C. I. Brannan, N. G. Copeland, N. A. Jenkins, S. Nagata, *Nature* **356**, 314 (1992).
16. T. Takahashi *et al.*, *Cell* **76**, 969 (1994).
17. M. Zörnig, A. Grzeschiczek, M. B. Kowalski, K. U. Hartmann, T. Möröy, *Oncogene* **10**, 2397 (1995).
18. A. O. Hueber and G. Evan, unpublished results.
19. A. Kauffmann-Zeh *et al.*, *Nature* **385**, 544 (1997).
20. N. J. McCarthy, M. K. B. Whyte, C. Gilbert, G. Evan, *J. Cell Biol.* **136**, 1 (1997).
21. A. Fanidi, E. A. Harrington, G. Evan, *Nature* **359**, 554 (1992); R. Bissonnette, F. Echeverri, A. Mahboubi, D. Green, *ibid.*, p. 552; A. J. Wagner, M. B. Small, N. Hay, *Mol. Cell Biol.* **13**, 2432 (1993).
22. N. Itoh, Y. Tsujimoto, S. Nagata, *J. Immunol.* **151**, 621 (1993).
23. I. Rodriguez *et al.*, *J. Exp. Med.* **183**, 1031 (1996).
24. J. Dhein, H. Walczak, C. Baumler, K. M. Debatin, P. H. Krammer, *Nature* **373**, 438 (1995).
25. R. P. Bissonnette, A. McGahon, A. Mahboubi, D. Green, *J. Exp. Med.* **180**, 2413 (1994).
26. Y. Shi *et al.*, *Science* **257**, 212 (1992).
27. B. Amati, T. Littlewood, G. Evan, H. Land, *EMBO J.* **12**, 5083 (1993).
28. R. U. Janicke, F. H. Lee, A. G. Porter, *Mol. Cell Biol.* **14**, 5661 (1994).
29. J. Klefstrom *et al.*, *EMBO J.* **13**, 5442 (1994).
30. S. Strand *et al.*, *Nature Med.* **2**, 1361 (1996).
31. M. Hahne *et al.*, *Science* **274**, 1363 (1996).
32. W. S. Pear, G. P. Nolan, M. L. Scott, D. Baltimore, *Proc. Natl. Acad. Sci. U.S.A.* **90**, 8392 (1993).
33. One hundred randomly picked live cells were selected at the start of the experiment and followed by time-lapse videomicroscopy at a rate of 12 frames per hour. At the end of each 2-hour time interval, the total number of apoptotic events thus far was summed and plotted as cumulative cell deaths versus time. Results obtained from the time-lapse videomicroscopy were confirmed by two independent cell death assays: propidium iodide exclusion, which monitors cell permeability, and the MTT assay, which assays mitochondrial function (8).
34. Total RNA was isolated from mouse thymus, S3T3 c-MycER cells, and MEF cells by use of the TRIzol reagent (Gibco/BRL). First-strand cDNA synthesis was performed with 2 μ g of RNA according to standard protocols. Five percent of this cDNA was used in a first-round polymerase chain reaction (PCR) with

Fig. 3. Myc, IGF-I, and Bcl-2 regulate the CD95 pathway. **(A)** Rat-1 cells become sensitive to CD95-induced apoptosis only after activation of c-Myc. Rat-1 c-MycER fibroblasts were grown in 2% FCS for 36 hours. CD95 killing was induced by addition of a soluble CD95 ligand molecule (CD95Ls; Alexis Corporation) at 25 or 100 ng/ml. c-Myc was activated by addition of 4-OHT. **(B)** IGF-I protects S3T3 cells against CD95-mediated killing. S3T3 MycER fibroblasts were deprived of serum for 48 hours, and anti-mouse CD95 (Jo2; 4 ng/ml) was then added to the culture in the presence (100 ng/ml) or absence of IGF-I; the cells were then analyzed for cell death by time-lapse videomicroscopy. **(C)** Bcl-2 protects S3T3 cells against CD95-induced apoptosis. S3T3 cells stably infected with vector alone (pB Hygro) or with pBabe Hygro Bcl-2 (pB Hygro Bcl-2) were serum-deprived for 48 hours. Anti-mouse CD95 (Jo2; 100 ng/ml) was then added, and the cultures were analyzed for cell death by time-lapse videomicroscopy.



the primer pair CD95L1 and CD95L2 (1 μ M each). Reaction conditions were as follows: one cycle at 94°C for 3 min; 40 cycles at 95°C for 1 min, at 65°C for 1 min 30 s, and at 72°C for 2 min; and one cycle at 72°C for 8 min. Two microliters of a 1:10 dilution of the amplification product served as a template for a second round of PCR amplification with the nested primer pair CD95L3 and CD95L4 (1 μ M each). Reaction conditions: one cycle for 3 min at 94°C; 40 cycles at 95°C for 1 min, at 55°C for 1 min 30 s, and at 72°C for 2 min; and one cycle at 72°C for 8 min. A portion of the amplification product was blotted on a nylon membrane and hybridized with the γ -³²P-labeled internal oligonucleotide CD95L5. A single round of PCR amplification was carried out with 2 μ l of cDNA and the primer pair Act1 and Act2 (1 μ M each). Reaction conditions were identical to those used in the first-round PCR. Primer sequences: CD95L1, 5'-GTATTTTTCATGGTCTGGTGG-3'; CD95L2, 5'-ATGAATCC-

TGGTGCCCATG-3'; CD95L3, 5'-AAGCTTCAGCTC-TTCCACCTG-3'; CD95L4, 5'-TAAAGAATAGTAGAT-CATTT-3'; CD95L5, 5'-AAGTATACTCCGGGGTC-AGT-3'; Act1, 5'-GTGGCCATCTCCTGCTCGAAGTC-3'; and Act2, 5'-GTTTGAGACCTTCAACACCCC-3'.
 35. T. Suda and S. Nagata, unpublished data.
 36. The Fadd dominant-negative molecule [FADD(80-208)] (11) was cloned into the retroviral expression vector pBabe Hygro and transfected into the retroviral packaging cell line GP+E. Recombinant retrovirus was harvested 48 hours later and used to infect S3T3 c-MycER cells in the presence of polybrene (8 μ g/ml). Control retrovirus was prepared by transfecting the GP+E packaging line with pBabe Hygro vector alone. Cells were selected with Hygromycin (Sigma; 200 μ g/ml), and resistant cells were pooled.
 37. The pBabe puro c-MycER construct was transfected into the retroviral packaging cell line BOSC (32). Recombinant retrovirus was harvested 48

hours later and used to infect MEFs prepared from WT, *lpr*, or *gld* embryos in the presence of polybrene (8 μ g/ml). Twenty-four hours after infection, the medium was replaced and the cells were cultivated in 0.5% FCS in the presence or absence of OHT.

38. We thank A. M. Bernard and M. Chautan for providing *lpr* MEFs; V. Dixit for providing the mutant DN Fadd construct; P. Golstein for the L12.10 CD95 cells; T. Mörry, T. Schmidt, and H. Karsunky for help and support with the MEF experiments; and our colleagues at ICRF for advice and criticism. A.-O.H. is supported by a fellowship from the European Molecular Biology Laboratory and M.Z. by a Marie Curie TMR Fellowship (ERBFMBICT 950498) from the European Community (EC). We are grateful for support from MRC-LINK G9321238.EC and from EC grants BioTech BIO4-CT96-0052 and BioMed2 BMH4-CT96-0010.

22 July 1997; accepted 3 October 1997

A TEL-JAK2 Fusion Protein with Constitutive Kinase Activity in Human Leukemia

Virginie Lacronique, Anthony Boureux, Véronique Della Valle, Hélène Poiriel, Christine Tran Quang, Martine Mauchauffé, Christian Berthou, Michel Lessard, Roland Berger, Jacques Ghysdael, Olivier A. Bernard*

The Janus family of tyrosine kinases (JAK) plays an essential role in development and in coupling cytokine receptors to downstream intracellular signaling events. A t(9;12)(p24;p13) chromosomal translocation in a T cell childhood acute lymphoblastic leukemia patient was characterized and shown to fuse the 3' portion of *JAK2* to the 5' region of *TEL*, a gene encoding a member of the ETS transcription factor family. The TEL-JAK2 fusion protein includes the catalytic domain of *JAK2* and the TEL-specific oligomerization domain. TEL-induced oligomerization of TEL-JAK2 resulted in the constitutive activation of its tyrosine kinase activity and conferred cytokine-independent proliferation to the interleukin-3-dependent Ba/F3 hematopoietic cell line.

analyze RNA from leukemic or control cells by reverse transcriptase (RT)-PCR (10). Both TEL-JAK2 and JAK2-TEL cDNAs were specifically amplified from patient cells but not from control cells (Fig. 1C). The sequence of the amplified human *JAK2* was 90% identical to that of murine *Jak2* at the nucleotide level and 96% identical at the protein level over a stretch of 114 amino acids (Fig. 2A). These results establish that human *JAK2* is the gene fused to *TEL* as a result of the t(9;12) translocation.

JAK2 is a widely expressed protein tyrosine kinase that associates with the intracellular domains of a number of cytokine receptors and is essential to receptor function (11, 12). *JAK2* shares with other members of the JAK family (such as *JAK1*, *JAK3*, and *TYK2*) seven regions of homology, referred to as JH1 to JH7 (Fig. 2C) (11, 13). JH1 is the catalytic domain, whereas JH2 to JH7 appear to be involved in protein-protein interactions and in the specificity of the different JAK family members (14, 15). In the TEL-JAK2 fusion, the NH₂-terminal TEL sequences are fused to the kinase JH1 domain (Fig. 2C). TEL is a member of the ETS family of transcription factors. In addition to a COOH-terminal ETS domain that is conserved in all ETS proteins, TEL specifically contains a 60-amino acid homotypic oligomerization domain at its NH₂-terminus (16, 17). Fusion of *TEL* and *JAK2* has been observed in two other leukemic patients, which also resulted in a TEL-JAK2 fusion transcript but not in the expression of the reciprocal JAK2-TEL fusion (Fig. 2B) (18). The conserved feature of the fusion proteins encoded by the TEL-JAK2 transcripts characterized in all three patients is the presence of both the TEL oligomerization domain and the *JAK2* catalytic domain (Fig. 2C).

To investigate the oligomerization properties and protein kinase activity of TEL-JAK2, we compared the properties of intact TEL-JAK2, in which the 336 NH₂-terminal residues of TEL are fused to 318 COOH-

Chromosomal translocations in human tumors frequently produce fusion genes whose chimeric protein products play an essential role in oncogenesis (1). *TEL* is located on chromosome 12p13 and is frequently involved in chromosomal translocations seen in a variety of human leukemias (2-4). We observed a t(9;12)(p24;p13) translocation in a 4-year-old male with T cell acute lymphoblastic leukemia (ALL) in relapse (Fig. 1A). The involvement of *TEL* was investigated by Southern (DNA) blot analysis with a genomic probe corresponding to intron 5 of *TEL* (5, 6). In addition to the expected germline bands, rearranged frag-

ments were detected in the Eco RI and Bam HI digests of the patient's DNA, suggesting that the chromosome 12 breakpoint localized to TEL intron 5 (Fig. 1B). To identify the fusion partner on chromosome 9, we used anchored polymerase chain reaction (PCR) to characterize the fusion transcript in leukemic cells. Sequence analysis of the amplified cDNA clones identified a non-TEL sequence fused in frame upstream of TEL exon 6. This sequence showed extensive similarity to the genes encoding the JAK family of protein tyrosine kinases, with the greatest similarity to murine *Jak2* (7).

Using these putative *JAK2* cDNA sequences, we isolated lambda phage clones from a normal human genomic library and showed by fluorescent in situ hybridization (FISH) that they hybridized to chromosome 9p24 (8), the chromosomal location of human *JAK2* (9). Partial sequence analysis of these genomic clones allowed us to design *JAK2* oligonucleotides corresponding to sequences on either side of the chromosome 9 breakpoint. These oligonucleotides were used together with TEL-specific primers to

V. Lacronique, V. Della Valle, H. Poiriel, M. Mauchauffé, R. Berger, O. A. Bernard, U 301 de l'Institut National de la Santé et de la Recherche Médicale and SD 401 No. 301 CNRS, Institut de Génétique Moléculaire, 27 rue Juliette Dodu, 75010 Paris, France.

A. Boureux, C. Tran Quang, J. Ghysdael, CNRS Unité Mixte de Recherche 146, Institut Curie-Section de Recherche, Centre Universitaire, 91405 Orsay Cedex, France.

C. Berthou and M. Lessard, Unité d'Hématologie, Laboratoire de Cytogénétique, Hôpital Morvan, Centre Hospitalier Régional de Brest, 29609 Brest Cedex, France.

*To whom correspondence should be addressed.